

Research Article

A Comparative Study on Improved Arrhenius-Type and Artificial Neural Network Models to Predict High-Temperature Flow Behaviors in 20MnNiMo Alloy

Guo-zheng Quan, Chun-tang Yu, Ying-ying Liu, and Yu-feng Xia

School of Material Science and Engineering, Chongqing University, Chongqing 400044, China

Correspondence should be addressed to Guo-zheng Quan; quangz3000@sina.com

Received 24 August 2013; Accepted 22 December 2013; Published 12 February 2014

Academic Editors: F. Berto and Y.-Y. Chen

Copyright © 2014 Guo-zheng Quan et al. This is an open access article distributed under the Creative Commons Attribution License, which permits unrestricted use, distribution, and reproduction in any medium, provided the original work is properly cited.

The stress-strain data of 20MnNiMo alloy were collected from a series of hot compressions on Gleeble-1500 thermal-mechanical simulator in the temperature range of 1173~1473 K and strain rate range of 0.01~10 s⁻¹. Based on the experimental data, the improved Arrhenius-type constitutive model and the artificial neural network (ANN) model were established to predict the high temperature flow stress of as-cast 20MnNiMo alloy. The accuracy and reliability of the improved Arrhenius-type model and the trained ANN model were further evaluated in terms of the correlation coefficient (R), the average absolute relative error (AARE), and the relative error (η). For the former, R and AARE were found to be 0.9954 and 5.26%, respectively, while, for the latter, 0.9997 and 1.02%, respectively. The relative errors (η) of the improved Arrhenius-type model and the ANN model were, respectively, in the range of -39.99%~35.05% and -3.77%~16.74%. As for the former, only 16.3% of the test data set possesses η -values within $\pm 1\%$, while, as for the latter, more than 79% possesses. The results indicate that the ANN model presents a higher predictable ability than the improved Arrhenius-type constitutive model.

1. Introduction

20MnNiMo is a low carbon steel with moderate strength, superior plasticity and toughness, good ductility and workability. Due to its low neutron irradiation sensitivity and superior performance, 20MnNiMo is increasingly and extensively applied in manufacture of large and medium-sized nuclear reactor pressure vessel [1]. The understanding of the flow behaviors of metals and alloys at a hot deformation condition has a great importance for designers engaged in metal forming (hot rolling, forging, extrusion, etc.), since flow behaviors have an effective role on material deformation pattern as well as on the kinetics of metallurgical transformation. The constitutive relationships are often used to describe the material deformation pattern in a form that can be used in computer codes to model the forging response of mechanical part under the prevailing loading conditions [2]. So far, Lee et al. [3] have investigated the influence of composition and distribution of carbides on the fracture toughness of 20MnNiMo steel.

Sun and his colleagues describe the mechanical responses and microstructural evolutions of the 20MnNiMo steel under various hot deformation conditions [4]. Nevertheless, there is still a lack of basic understanding of the hot deformation behavior of 20MnNiMo alloys until now [1, 3, 4]. Therefore, it is necessary to investigate high temperature flow behavior of 20MnNiMo alloy and accurately predict the stress.

Constitutive relationship is a mathematical representation for describing the correlation between flow stress, strain, strain rate and temperature in a wide range of working conditions [5, 6]. Many researchers have attempted to develop constitutive equations from the experimental data to accurately describe the thermal deformation behavior of materials [7–11]. And constitutive model expressed by the hyperbolic sine law has been extensively applied to describe the hot deformation behavior of materials. Various modifications of this model have also been suggested to improve its predictability [8–13]. Slooff et al. [11] introduced strain-dependent parameters in the hyperbolic sine constitutive

model to predict the flow stress in a wrought magnesium alloy. Lin et al. [12] developed the strain-dependent hyperbolic sine constitutive model by compensation of strain rate in Zener-Hollomon parameter ($Z = \dot{\epsilon} \exp(Q/RT)$) to predict flow behavior of 42CrMo steel, and the results showed that the strain-compensated Arrhenius-type equations could track the deformation behavior more accurately than the other equations. Later, an improved Arrhenius-type constitutive equation incorporating a series of polynomial functions for each coefficient followed by Lin's method was constructed to describe the high temperature flow behaviors of AZ81 magnesium alloy [13].

However, the improved Arrhenius-type constitutive model also has its own drawbacks in some certain cases such as low accuracy for predicting the relationships between flow stresses and processing variables and poor adaptability for the new experimental data [13, 14]. Recently, the artificial neural network (ANN) as an artificial intelligent approach was introduced to establish the constitutive relationship and further model the flow behaviors under hot compression of many metals and alloys [15–17]. Owing to its inherently high parallelism, ANN is ideally suited for the problem of estimating the flow stress from the available experimental data [16, 17]. It is in particular suitable for treating complex and nonlinear relationships and has been successfully applied to the prediction of constitutive relationships for some alloys [18]. More importantly, it is quite convenient to present the deformation behavior of materials with favorable accuracy under hot working conditions [19]. Xiao et al. [20] make a comparative study on the Arrhenius-type constitutive model considering strain compensation and artificial neural network models to predict the hot deformation behavior of the 12Cr3WV steel, and the results showed that the ANN model can predict the flow stress more efficient and accurate than the Arrhenius-type constitutive equations.

The objective of this investigation is to make a comparative study on the improved Arrhenius-type Constitutive model and artificial neural network models on their capability to predict the high-temperature flow behavior of 20MnNiMo alloy. Experimental data from isothermal hot compression tests on Gleeble-1500 thermal-mechanical simulator in a temperature range from 1173 K to 1473 K and a strain rate range from 0.01 s^{-1} to 10 s^{-1} are used to resolve the improved Arrhenius-type Constitutive model and to develop artificial neural network model. Subsequently, the suitability of these models to predict the elevated temperature flow behavior was evaluated based on the correlation coefficient (R), average absolute relative error (AARE), and relative error (η).

2. Materials and Experiment Procedures

The chemical compositions (wt%) of 20MnNiMo alloy were C-0.2, Si-0.16, Mn-1.53, S-0.0022, P-0.0063, Ni-0.81, Mo-0.57, Cr-0.14, V-0.005, Cu-0.04, and Fe (balance). Before the experiment, the extruded rod was homogenized under temperature 1523 K for 12 h. Then the rod was scalped to height 12 mm and diameter 10 mm with grooves on both sides filled

with machine oil mingled with graphite powder as lubricant to reduce friction between the anvils and specimen. On a computer-controlled, servohydraulic Gleeble-1500 machine, the specimens were resistance-heated at a heating rate of 10 K/s and held at a certain temperature for 180 s to ensure a uniform starting temperature and decrease the material anisotropy. Sixteen specimens were compressed with a height reduction of 60% at four different temperatures of 1173 K, 1273 K, 1373 K, and 1473 K and four different strain rates of 0.01 s^{-1} , 0.1 s^{-1} , 1 s^{-1} , and 10 s^{-1} . During the compressing process the variations of stress and strain were monitored continuously by a personal computer equipped with an automatic data acquisition system. The true stress-strain relationships were derived from the nominal stress-strain curves collected according to the following formula: $\sigma_T = |\sigma_N(1 + \epsilon_N)|$, $\epsilon_T = |\ln(1 + \epsilon_N)|$, where σ_T is the true stress, σ_N is the nominal stress, ϵ_T is the true strain, and ϵ_N is the nominal strain.

3. Results and Discussion

3.1. Flow Stress Behavior. The true stress-strain curves of 20MnNiMo alloy compressed at different deformation conditions are shown in Figures 1(a), 1(b), 1(c), and 1(d). The flow stress as well as the shape of the flow curves is sensitively dependent on strain rate and temperature. Comparing these curves with one another, it is found that, for a specific strain rate, the flow stress decreases markedly with temperature, while at a certain temperature, the flow stress generally increases as the strain rate increases due to an increase of dislocation density and the dislocation multiplication rate.

From the true stress-strain curves in Figures 1(a), 1(b), 1(c), and 1(d), it can be seen that the stress evolution with strain exhibits three distinct stages [21]. At the first stage, where work hardening (WH) predominates and causes dislocations to polygonize into stable subgrains, flow stress exhibits a rapid increase to a critical value with increasing strain, resulting in equiaxed DRX grains. At the second stage, flow stress exhibits a smaller and smaller increase until a peak value or an inflection of work-hardening rate, which shows that the thermal softening due to DRX and dynamic recovery (DRV) becomes more and more predominant, then it exceeds WH. At the third stage, three types of curve variation tendency can be generalized as follows: decreasing gradually to a steady state with DRX softening (1173~1473 K and 0.01 s^{-1} , 1373~1473 K, and 0.1 s^{-1}), maintaining higher stress level without significant softening and work-hardening (1173~1273 K and 0.1 s^{-1} , 1173~1373 K and 1 s^{-1} , 1173~1373 K and 10 s^{-1}), and increasing continuously with significant work hardening (1473 K and 1 s^{-1} , 1473 K and 10 s^{-1}). Thus, it can be concluded that the typical form of flow curve with DRX softening, including a single peak followed by a steady state flow as a plateau, is more recognizable at higher temperatures and lower strain rates. That is because at lower strain rates and higher temperatures, the higher DRX softening rate slows down the rate of work-hardening, and both the peak stress and the onset of steady state flow are therefore shifted to lower strain levels [22–27].

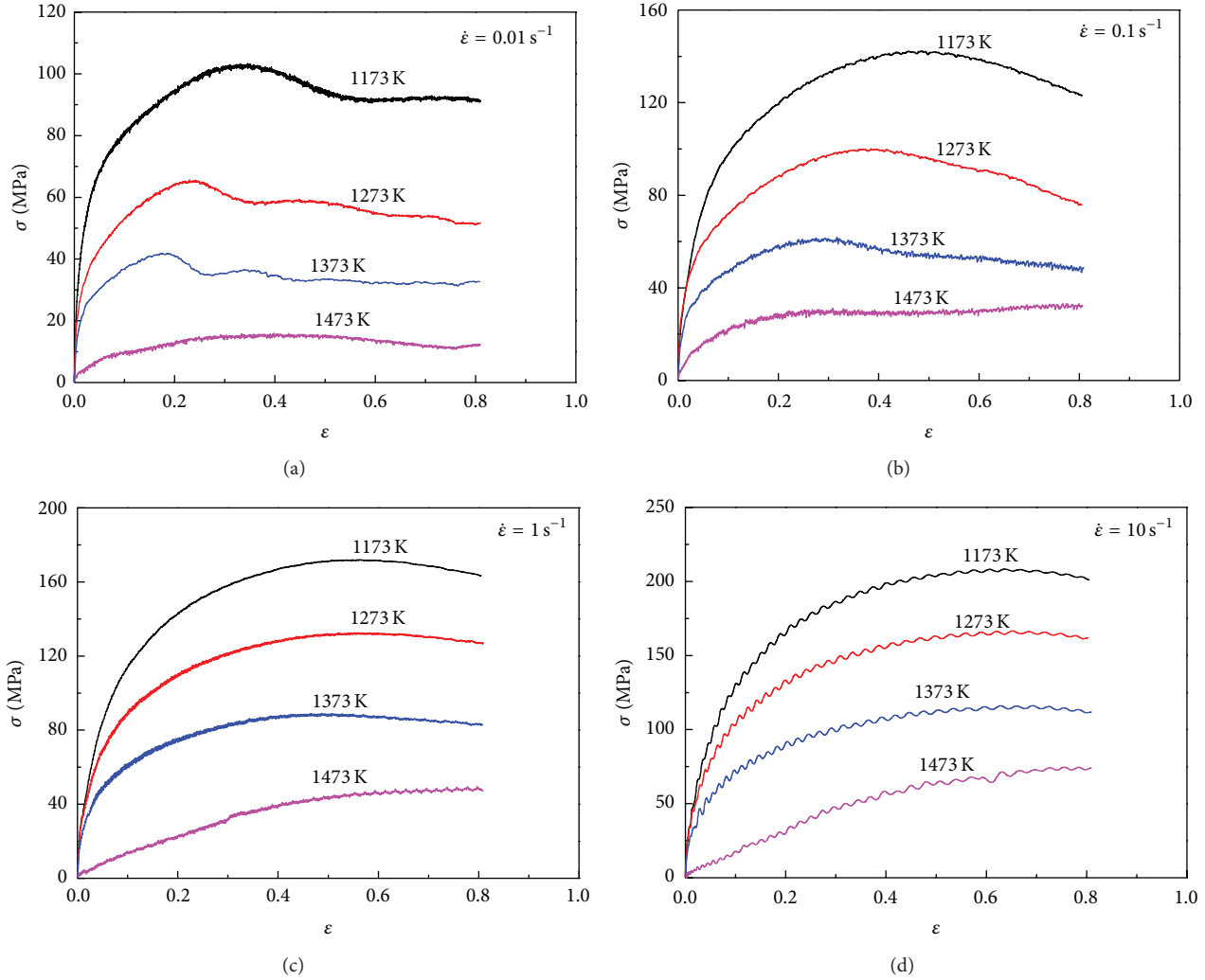


FIGURE 1: The true stress-strain curves of as-cast 20MnNiMo alloy under the different temperatures with strain rates (a) 0.01 s^{-1} , (b) 0.1 s^{-1} , (c) 1 s^{-1} , (d) 10 s^{-1} .

3.2. *Improved Arrhenius-Type Constitutive Model.* In order to further investigate the thermal deformation behaviors of 20MnNiMo alloy, it is necessary to study the constitutive characteristics. The stress-strain data obtained from hot compression tests can be used to determine the material constants of the constitution equation. The Arrhenius equation is widely used to describe the relationship between flow stress, deformation temperature, and strain rate, especially at high temperature [28]. Furthermore, the effects of deformation temperature and strain rate on the deformation behaviors can be represented by Zener-Hollomon parameter (Z) in an exponential equation [29]. The two equations are mathematically expressed as

$$Z = \dot{\epsilon} \exp(Q/RT). \tag{1}$$

$$\dot{\epsilon} = AF(\sigma) \exp(-Q/RT), \tag{2}$$

where,

$$F(\sigma) = \begin{cases} \sigma^n & \alpha\sigma < 0.8 \\ \exp(\beta\sigma) & \alpha\sigma > 1.2 \\ [\sinh(\alpha\sigma)]^n & \text{for all } \sigma \end{cases} \tag{3}$$

in which $\dot{\epsilon}$ is the strain rate (s^{-1}), R is the universal gas constant ($8.31 \text{ J}\cdot\text{mol}^{-1}\cdot\text{K}^{-1}$), T is the absolute temperature (K), Q is the activation energy of DRX ($\text{kJ}\cdot\text{mol}^{-1}$), σ is the flow stress (MPa) for a given strain, A , and α and n are the material constants, $\alpha = \beta/n$.

It is commonly accepted that the effect of strain on stress has not been considered in (1) and (2). Here the effects of deformation strain on stress are investigated by the consideration of the influence of strain on a series of variable coefficients (including activation energy of deformation Q , material constants n and α , and structure factor A) in Arrhenius type model. The following is taking the strain of 0.2 as an example.

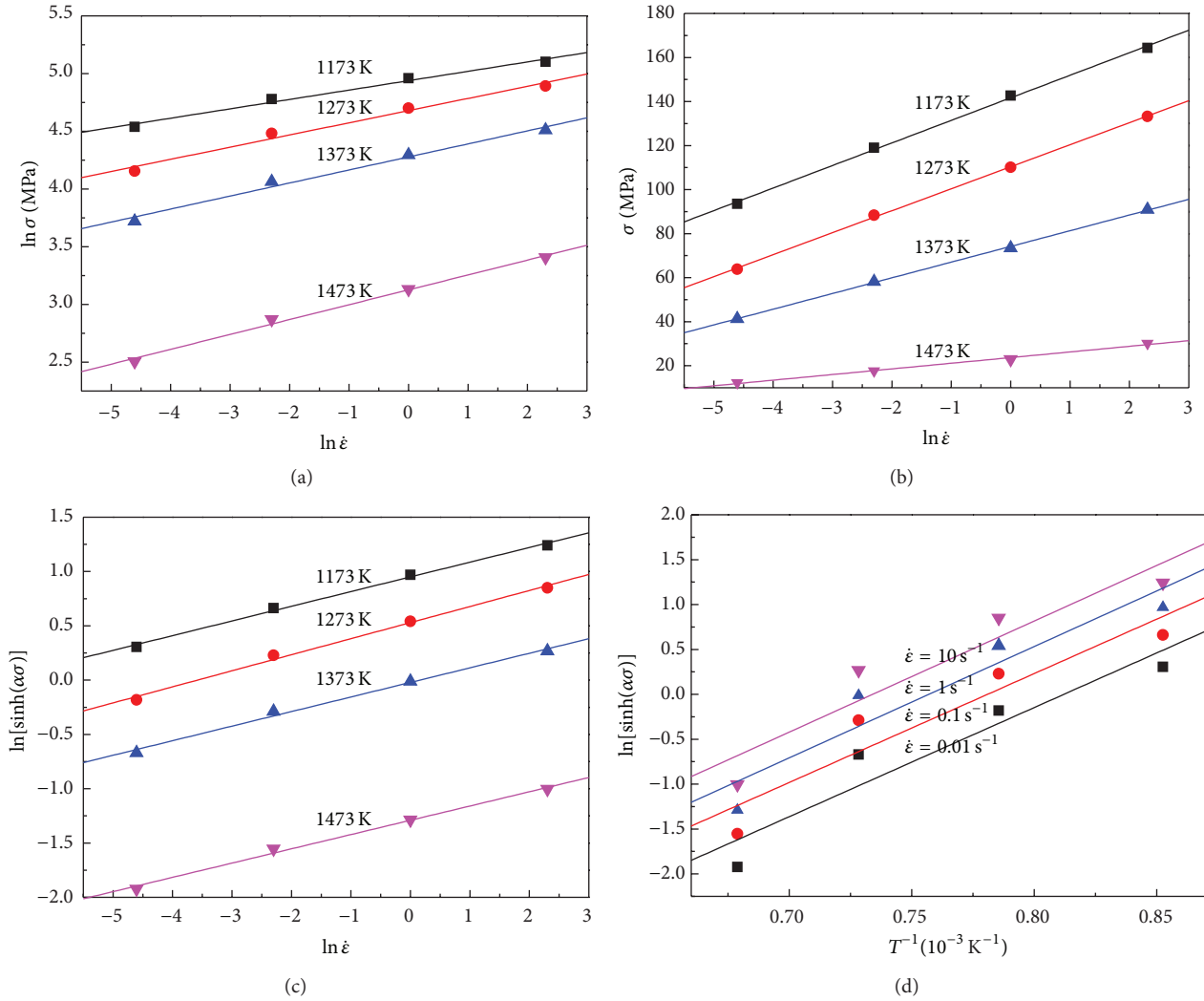


FIGURE 2: The relationships between (a) $\ln \sigma$ and $\ln \dot{\epsilon}$, (b) σ and $\ln \dot{\epsilon}$, (c) $\ln[\sinh(\alpha\sigma)]$ and T^{-1} , and (d) $\ln[\sinh(\alpha\sigma)]$ and $\ln \dot{\epsilon}$.

For the low stress level ($\alpha\sigma < 0.8$) and high stress level ($\alpha\sigma > 1.2$), by substituting power law and exponential law of $F(\sigma)$ into (2), the relationships between flow stress and strain rate can be expressed in the following equations, respectively,

$$\dot{\epsilon} = B\sigma^n \tag{4}$$

$$\dot{\epsilon} = B' \exp(\beta\sigma), \tag{5}$$

where B and B' are the material constants that are dependent of deformation temperatures. Taking natural logarithms on both sides of (4) and (5), respectively, gives

$$\ln \sigma = \frac{1}{\beta} \ln \dot{\epsilon} - \frac{1}{\beta} B', \tag{6}$$

$$\sigma = \frac{1}{\beta} \ln \dot{\epsilon} - \frac{1}{\beta} B'. \tag{7}$$

Then, $1/n = d \ln \sigma / d \ln \dot{\epsilon}$ and $1/\beta = d\sigma / d \ln \dot{\epsilon}$. Substituting the values of the flow stress and corresponding

strain rate at the strain of 0.2 into the logarithms (6) and (7) gives the relationship between stress and strain rate as shown in Figure 2. Figures 2(a) and 2(b) show the relationships of $\sigma - \ln \dot{\epsilon}$ and $\ln \sigma - \ln \dot{\epsilon}$ for $\epsilon = 0.2$ at the temperatures of 1173 K, 1273 K, 1373 K, and 1473 K. In Figure 2(a) the average value of all the lines' slopes is equal to the inverse of n -value, thus $n = 7.30547 \text{ MPa}^{-1}$ for $\epsilon = 0.2$. Meanwhile in Figure 2(b) the average value of all the lines' slopes is equal to the inverse of β -value, thus $\beta = 0.098854 \text{ MPa}^{-1}$ for $\epsilon = 0.2$. Then $\alpha = \beta/n = 0.0011897$.

For all the stress level (including low and high-stress levels), (2) can be represented as follows:

$$\dot{\epsilon} = A[\sinh(\alpha\sigma)]^n \exp(-Q/RT). \tag{8}$$

By substituting Zener-Hollomon parameter $Z = \dot{\epsilon} \exp(Q/RT)$ into (8), the flow stress can be expressed as follows (9):

$$\sigma = \frac{1}{\alpha} \ln \left\{ \left(\frac{Z}{A} \right)^{1/n} + \left[\left(\frac{Z}{A} \right)^{2/n} + 1 \right]^{1/2} \right\}. \tag{9}$$

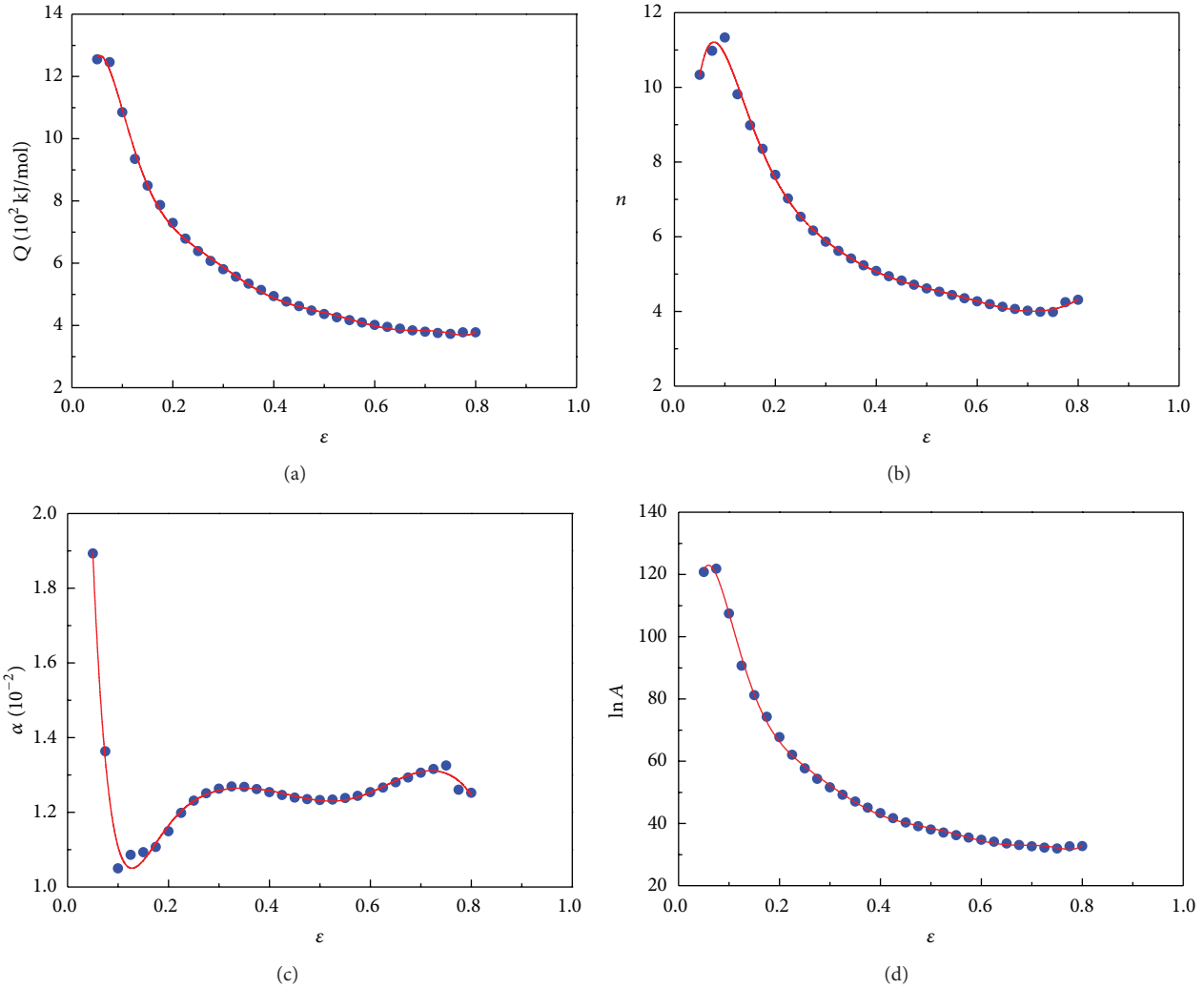


FIGURE 3: Relationship between (a) Q , (b) n , (c) α , (d) $\ln A$ and true strain by polynomial fit of 20MnNiMo alloy.

Taking the logarithm of both sides of (8) gives

$$\ln \sinh(\alpha\sigma) = \frac{1}{n} \ln \dot{\epsilon} + \frac{Q}{nRT} - \frac{1}{n} \ln A. \quad (10)$$

For the fixed temperature and strain, by differentiating (10), the value of n can be expressed as

$$\frac{1}{n} = \frac{d \ln \sinh(\alpha\sigma)}{d \ln \dot{\epsilon}}. \quad (11)$$

The value of n can be obtained from the slope in a plot of $\ln \sinh(\alpha\sigma) - \ln \dot{\epsilon}$ by substituting the values of the flow stress and strain rate for all the tested temperatures into (11) and the linear relationships between $\ln \sinh(\alpha\sigma)$ and $\ln \dot{\epsilon}$ at different temperatures were fitted out as Figure 2(c). The mean value of all the intercepts of $\ln \sinh(\alpha\sigma)$ versus $\ln \dot{\epsilon}$ plots is accepted as A value; furthermore A value for $\epsilon = 0.2$ is obtained as $3.769 \times 10^{12} \text{ s}^{-1}$.

For the given strain rate conditions, differentiating (10) gives

$$Q = Rn \left\{ \frac{d [\ln \sinh(\alpha\sigma)]}{d (1/T)} \right\}. \quad (12)$$

It is clear that the value of Q can be derived from the slope in a plot of $\ln[\sinh(\alpha|\sigma|)]$ as a function of $1/T$ as shown in Figure 2(d). From a group of parallel and straight lines in Figure 2(d), the value of activated energy (Q) as 744.34 kJ/mol can be easily evaluated by averaging the values of (Q) under different strain rates.

Then, the values of material constants (Q , n , $\ln A$, and α) of the constitutive equations were computed under different deformation strains within the range of 0.05~0.80 and the interval of 0.025. The relationships between, Q , n , $\ln A$, α , and true strain for 20MnNiMo alloy (Figure 3) can be polynomially fitted by the compensation of strain, as shown in (13). The

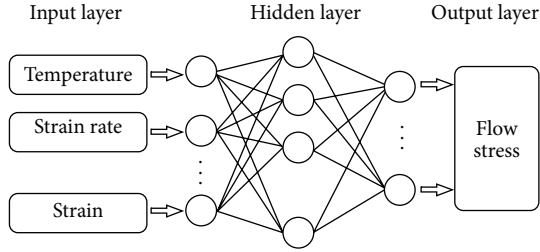


FIGURE 4: Schematic illustration of the neural network architecture.

polynomial fit results of Q , n , $\ln A$, and α of 20MnNiMo alloy are provided in Table 1. Consider the following:

$$\begin{aligned}
 Q &= j(\varepsilon) = B_0 + B_1\varepsilon + B_2\varepsilon^2 + B_3\varepsilon^3 + B_4\varepsilon^4 \\
 &\quad + B_5\varepsilon^5 + B_6\varepsilon^6 + B_7\varepsilon^7 + B_8\varepsilon^8 + B_9\varepsilon^9 \\
 n &= h(\varepsilon) = C_0 + C_1\varepsilon + C_2\varepsilon^2 + C_3\varepsilon^3 + C_4\varepsilon^4 \\
 &\quad + C_5\varepsilon^5 + C_6\varepsilon^6 + C_7\varepsilon^7 + C_8\varepsilon^8 + C_9\varepsilon^9 \\
 \ln A &= \ln f(\varepsilon) = D_0 + D_1\varepsilon + D_2\varepsilon^2 + D_3\varepsilon^3 \\
 &\quad + D_4\varepsilon^4 + D_5\varepsilon^5 + D_6\varepsilon^6 + D_7\varepsilon^7 + D_8\varepsilon^8 + D_9\varepsilon^9 \\
 \alpha &= g(\varepsilon) = E_0 + E_1\varepsilon + E_2\varepsilon^2 + E_3\varepsilon^3 + E_4\varepsilon^4 \\
 &\quad + E_5\varepsilon^5 + E_6\varepsilon^6 + E_7\varepsilon^7 + E_8\varepsilon^8 + E_9\varepsilon^9.
 \end{aligned} \tag{13}$$

Substituting Q , n , $\ln A$, and α in (14) into (8) gives the relationships between $\dot{\varepsilon}$, T , and σ as follows (14):

$$|\dot{\varepsilon}| = f(\varepsilon) \{ \sinh [g(\varepsilon) |\sigma|] \}^{h(\varepsilon)} \times \exp \left(\frac{j(\varepsilon)}{8.31T} \right). \tag{14}$$

Thus, $Z = |\dot{\varepsilon}| \exp [j(\varepsilon)/8.31T]$. Furthermore, the constitutive equation for flow behavior of 20MnNiMo alloy in a wide strain range of 0.05~0.80 can be expressed as follows (15):

$$\begin{aligned}
 |\sigma| &= \frac{1}{g(\varepsilon)} \ln \left\{ \left(\frac{|\dot{\varepsilon}| \exp [j(\varepsilon)/8.314T]}{f(\varepsilon)} \right)^{1/h(\varepsilon)} \right. \\
 &\quad \left. + \left[\left(\frac{|\dot{\varepsilon}| \exp [j(\varepsilon)/8.314T]}{f(\varepsilon)} \right)^{2/h(\varepsilon)} + 1 \right]^{1/2} \right\},
 \end{aligned} \tag{15}$$

where $j(\varepsilon)$, $h(\varepsilon)$, $f(\varepsilon)$, and $g(\varepsilon)$ are the polynomial functions of Q , n , A , and α at different true strains, and their expressions are as (13) and Table 1.

3.3. Artificial Neural Model. Artificial neural network (ANN) is a powerful treatment system for data information, which can mimic complex and nonlinear relationships through the application of many nonlinear processing units called neurons. A typical artificial neural networks architecture consists of an input layer, an output layer, and a hidden layer.

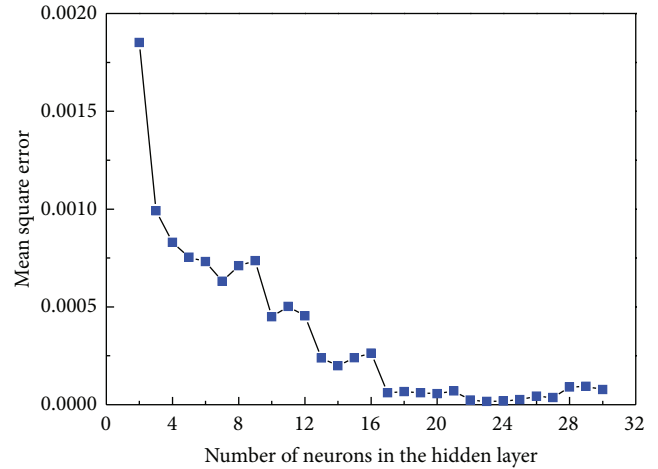


FIGURE 5: Influence of hidden neutrons on the network performance.

Some neuron serves the input variables, some provide the output, and the rest of the neurons remain hidden [30]. Back-propagation algorithm is the typical means of adjusting the weights and biases by utilizing gradient descent to minimize the target error, which is approximated in the vector space created by the weights and biases [31, 32]. Hence, a three-layer feed forward back-propagation (BP) artificial neural network (as shown in Figure 4) was employed to predict the hot deformation behavior of 20MnNiMo alloy in present work. The inputs of the ANN model are strain, log strain rate, and temperature. The output of the ANN model is flow stress.

When developing the ANN model, 396 random data sets from the true stress-true strain curves were used to train the network model, and 100 data sets at true strain between 0.05 and 0.80 with interval of 0.025 were applied to test the predictability of the ANN model. Before training the network, both input and output variable datasets were scaled between 0 and 1 in order to ensure that each variable lay in the same range during the training and the testing. The following equation was used widely for unification of data T , ε , and σ [25]:

$$X' = \frac{X - 0.95X_{\min}}{1.05X_{\max} - 0.95X_{\min}}, \tag{16}$$

where X is the original data, X_{\min} and X_{\max} are the minimum and maximum value of X , respectively, and X' is the unified data of the corresponding X . Since the $\dot{\varepsilon}$ changed sharply and the minimum value of $\dot{\varepsilon}$ after unification was too small for the ANN model to learn, the following equation is developed to unify the value of $\dot{\varepsilon}$:

$$\dot{\varepsilon}' = \frac{(3 + \lg \dot{\varepsilon}) - 0.95(3 + \lg \dot{\varepsilon}_{\min})}{1.05(3 + \lg \dot{\varepsilon}_{\max}) - 0.95(3 + \lg \dot{\varepsilon}_{\min})} \tag{17}$$

in which a constant 3 is defined to make the unified data be positive [25]. The transfer functions were “tan sigmoid”, and the training function was “Trainlm”.

In order to determine the appropriate number of neurons in the hidden layer, the trial-and-error procedure was started

TABLE I: Coefficients of the polynomial for Q , n , $\ln A$, and α .

Q		n		ln A		α	
B_0	3.65102	C_0	-0.679	D_0	11.623	E_0	5.15944
B_1	435.05898	C_1	426.108	D_1	5075.860	E_1	-111.124
B_2	-7461.731	C_2	-5647.043	D_2	-83266.642	E_2	1222.173
B_3	58435.579	C_3	36439.007	D_3	636234.990	E_3	-7277.770
B_4	-260734.696	C_4	-138689.722	D_4	-2791840	E_4	26505.195
B_5	712681.632	C_5	331449.121	D_5	7541680	E_5	-61800.962
B_6	-1215160	C_6	-503008.253	D_6	-12749000	E_6	92570.232
B_7	1260820	C_7	470572.854	D_7	13142600	E_7	-86054.036
B_8	-728384.449	C_8	-247492.493	D_8	-7554410	E_8	45145.823
B_9	179648.777	C_9	55999.977	D_9	1855720	E_9	-10212.362

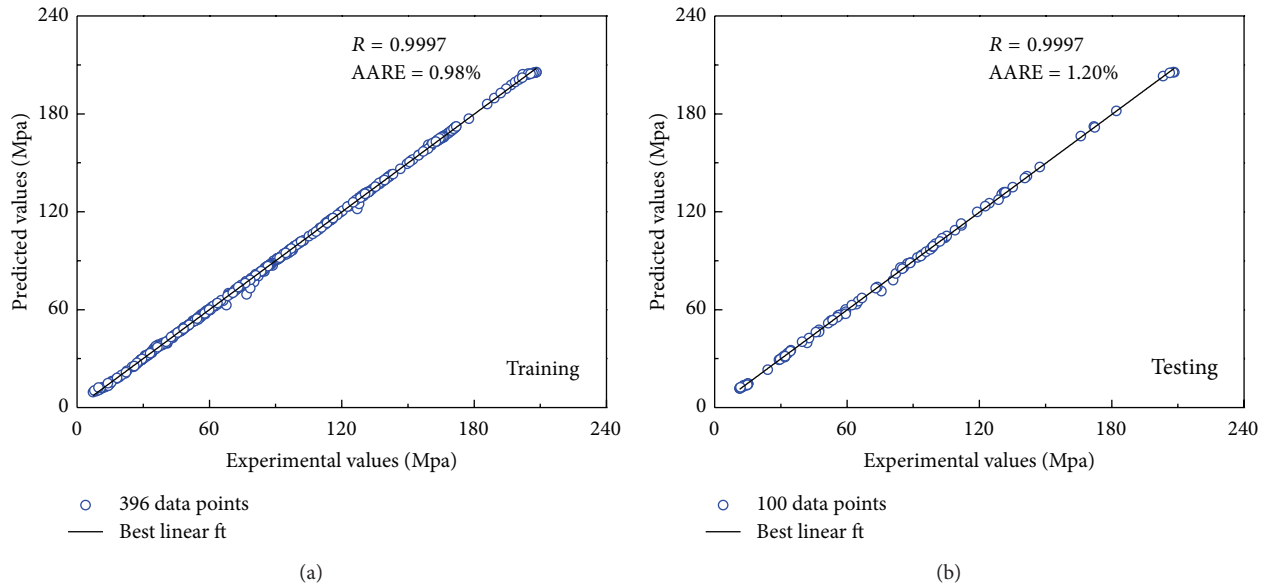


FIGURE 6: Correlation between the experimental and ANN predicted data for the (a) training and (b) test data.

with two neurons in the hidden layer and further carried out with more neurons. Figure 5 shows the influence of number of neurons in the hidden layer on the network performance. The value of mean square error is applied to check the ability of a particular architecture. It is founded that the value of mean square error decreases to the minimum value when the number of neurons is 23, which indicates that the network with 23 hidden neurons was the optimal structure for the prediction of flow stress of 20MnNiMo alloy.

Meanwhile, an evaluator, correlation coefficient (R) and average absolute relative error (AARE) are introduced in training and testing datasets to evaluate the performance of the ANN training work. These are defined as follows [18]:

$$R = \frac{\sum_{i=1}^N (E_i - \bar{E})(P_i - \bar{P})}{\sqrt{\sum_{i=1}^N (E_i - \bar{E})^2 \sum_{i=1}^N (P_i - \bar{P})^2}} \quad (18)$$

$$\text{AARE} (\%) = \frac{1}{N} \sum_{i=1}^N \left| \frac{E_i - P_i}{E_i} \right| \times 100,$$

where E is the sample of experimental value, P is the sample of predicted value by ANN model, \bar{E} and \bar{P} are the mean value of E and P , respectively, and N is the number of strain-stress samples. Comparisons of ANN with 23 hidden neurons predicted flow stress with experimental ones during training and testing are shown in Figures 6(a) and 6(b). Standard statistical performance indices of the ANN model during training, R and AARE, are 0.9997 and 0.98%; and those of test, R and AARE, are 0.9997 and 1.02%, respectively. These observations indicate that the trained ANN model with 23 hidden neurons has good capability to predict and generalize the hot deformation behavior of 20MnNiMo alloy.

3.4. Comparative Evaluation of the Improved Arrhenius-Type Constitutive Equations and the ANN Model. Figure 7 shows comparisons of the experimental flow stress data with values calculated by improved Arrhenius-type model for the four different temperatures under strain rates of 0.01 s^{-1} , 0.1 s^{-1} , 1 s^{-1} , and 10 s^{-1} . It can be easily found that the case of high strain rate of 1 s^{-1} and 10 s^{-1} is the best ideal one, and the

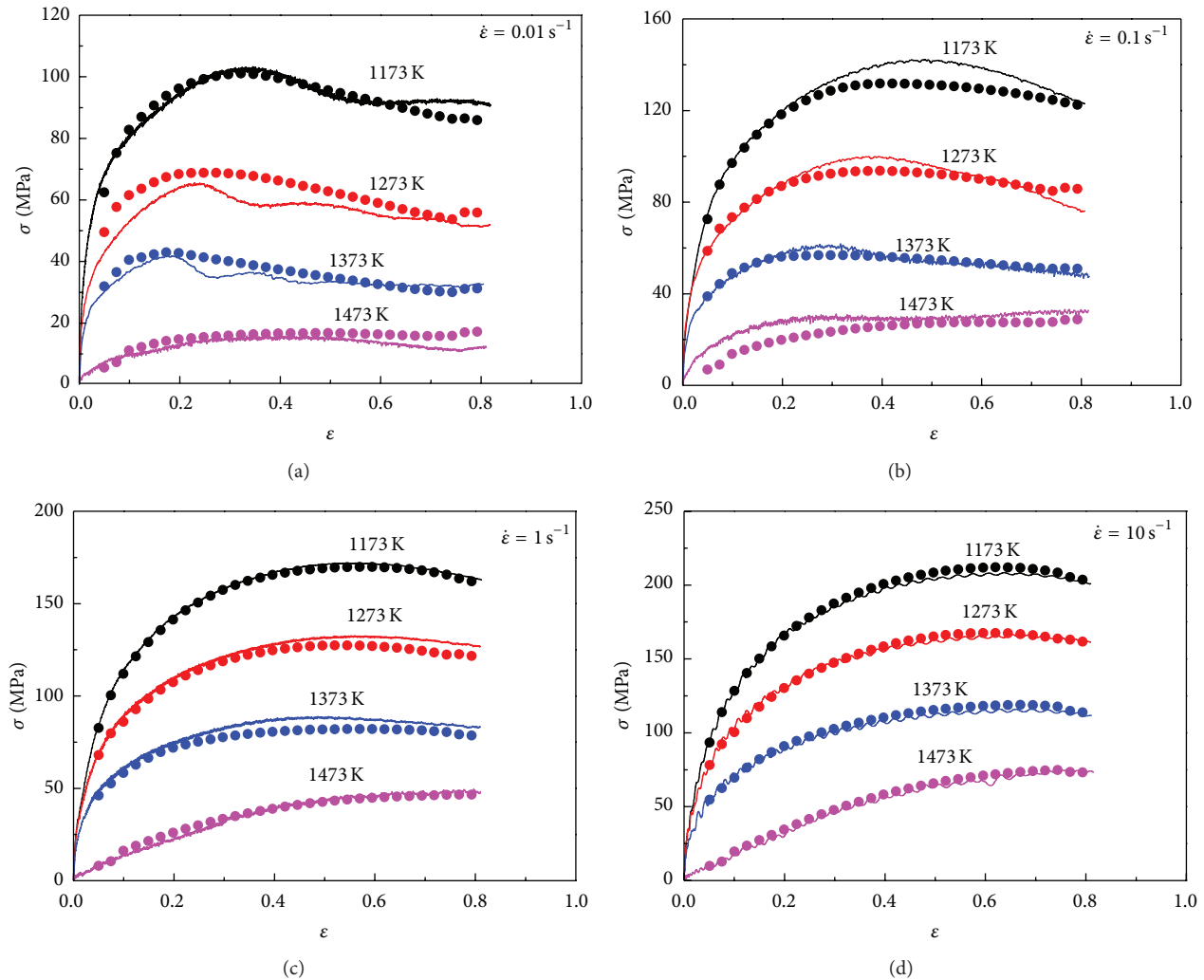


FIGURE 7: Comparison between the experimental and predicted flow stress by improved Arrhenius-type constitutive model at different strain rates and temperatures (a) 0.01 s^{-1} , (b) 0.1 s^{-1} , (c) 1 s^{-1} , and (d) 10 s^{-1} .

experimental and predicted results are in good agreement. However, for the case of low strain rates of 0.01 s^{-1} and 0.1 s^{-1} , there are obvious errors between the experimental and predicted results. The predicted flow stress is larger than the experimental one for the temperatures of 1273 K, 1373 K, and 1473 K at the strain rate of 0.01 s^{-1} , while the contrary conclusion will be obtained for the temperature of 1173 K and 1473 K at the strain rate of 0.1 s^{-1} . Furthermore, the predicted flow stress can not accurately describe the DRX characteristic very well.

The predicted flow stresses from ANN model and corresponding experimental ones at different temperatures and strain rates are compared as shown in Figure 8. It could be observed that the predicted values can track the experimental results very well throughout both the work hardening stage and dynamic softening stage (whatever it is DRX or DRV softening mechanism) in a wide temperature range of 1173~1473 K, a wide strain rate range of $0.01\sim 10 \text{ s}^{-1}$, and a wide strain range of $0.05\sim 0.8$. All above suggests that the present

ANN model has an excellent capability and high accuracy to describe the flow behavior of 20MnNiMo at different temperature and strain rates.

The accuracy of the improved Arrhenius-type constitutive equations and the ANN model was further quantified by the correlation coefficient (R) and the average absolute relative error (AARE). They can be expressed as (18). Figure 9 shows the plots of experimental values and predicted values predicted by improved Arrhenius-type constitutive equations and the ANN model, respectively. It is clearly seen that most of the data points lie very close to the line, and the correlation coefficients (R) for the Improved Arrhenius-type and ANN models are 0.9954 and 0.9997, respectively. The average absolute relative error (AARE) of the Improved Arrhenius-type model is 5.26%, which is larger than the value 1.02% of the ANN model.

The accuracy of the improved Arrhenius-type constitutive equations and the ANN model was further investigated by statistical analysis of the relative errors (η) between

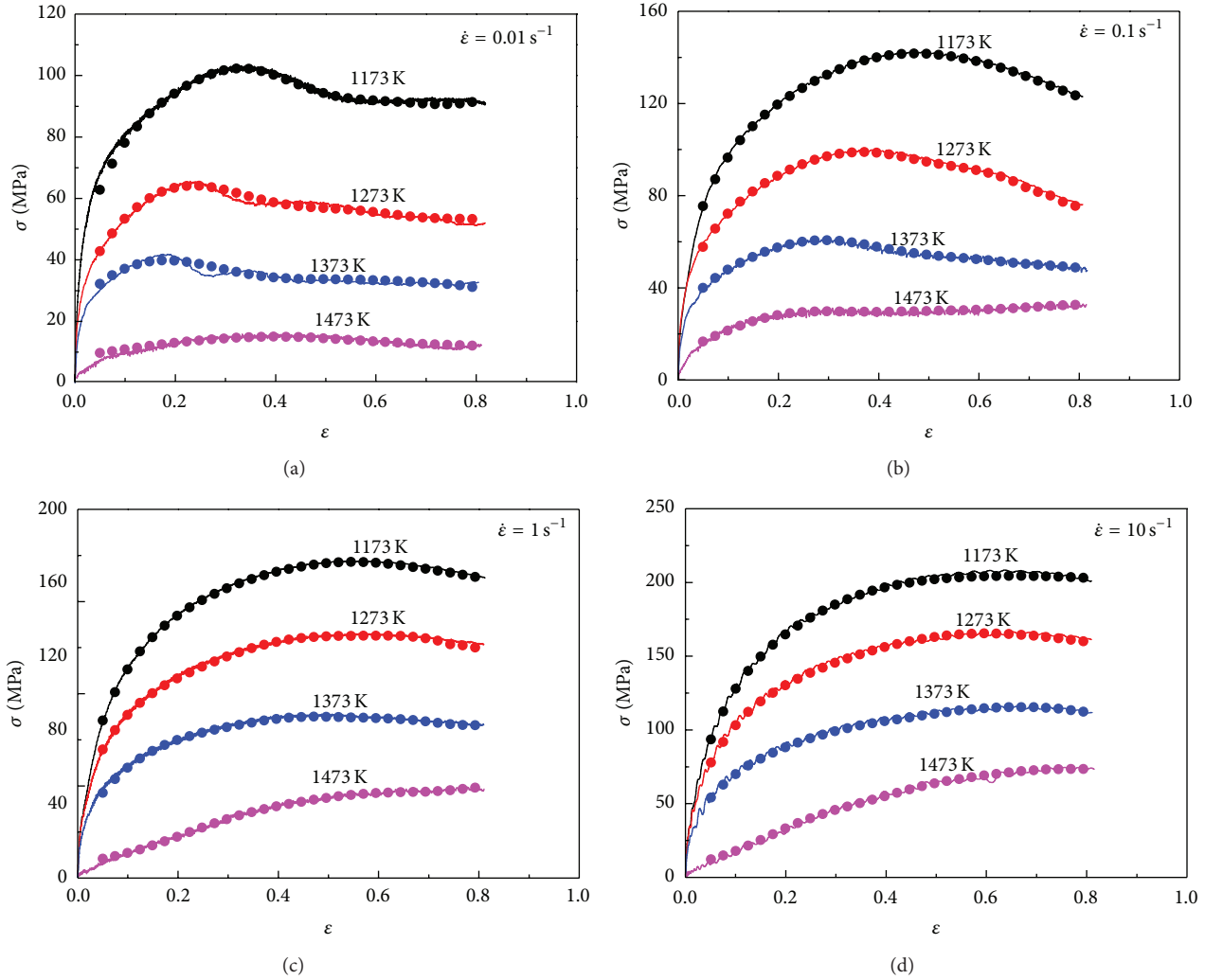


FIGURE 8: Comparison between the experimental and predicted flow stress by ANN model at different strain rates and temperatures (a) 0.01 s⁻¹, (b) 0.1 s⁻¹, (c) 1 s⁻¹, and (d) 10 s⁻¹.

the experimental values and predicted values, which were calculated by (19) as follows:

$$\eta (\%) = \frac{P_i - E_i}{E_i} \times 100\%, \quad (19)$$

where E is the sample of experimental value, P is the sample of predicted value by one model, and N is the number of strain-stress samples. Figure 10 shows the relative errors (η) of two models depicted as relative frequency versus relative error plot. It can be seen that the constitutive equations are in the range of $-39.99\% \sim 35.05\%$; whereas those are found to vary from -3.77% to 16.74% for the ANN model. Meanwhile, the relative error (η) within $\pm 1\%$ was observed for more than 79% of predicted data set of the ANN model while only for 16.3% of the predicted data sets for the constitutive equations, which reveals the higher accuracy of the ANN model.

All the results obtained above obviously indicate that the established ANN model showed good performance and could be applied to predict the flow behavior of 20MnNiMo alloys more accurately than the Improved Arrhenius-type models.

This is because the response of deformation behaviors of the materials under elevated temperatures and strain-rates is highly nonlinear, and many factors affecting the flow stress are also nonlinear, which make the prediction accuracy of the flow stress by the constitutive equations low and the applicable range limited [31, 32].

3.5. Prediction Potentiality of ANN Model Outside the Experimental Condition. It is well known that the well-trained ANN models could provide highly accurate prediction of flow stress over a wider range of temperatures and strain rates. Figures 11(a), 11(b), and 11(c) show the 3D surface plots representing the relationships of predicted flow stress versus strain and temperature, strain and log strain rate and temperature, respectively, at a fixed log strain rate of -1.5 , temperature of 1223 K, and strain of 0.5. Each node of the surface plots represents a data predicted by ANN model and most of the predicted data were outside the experimental conditions. From Figure 11 it can

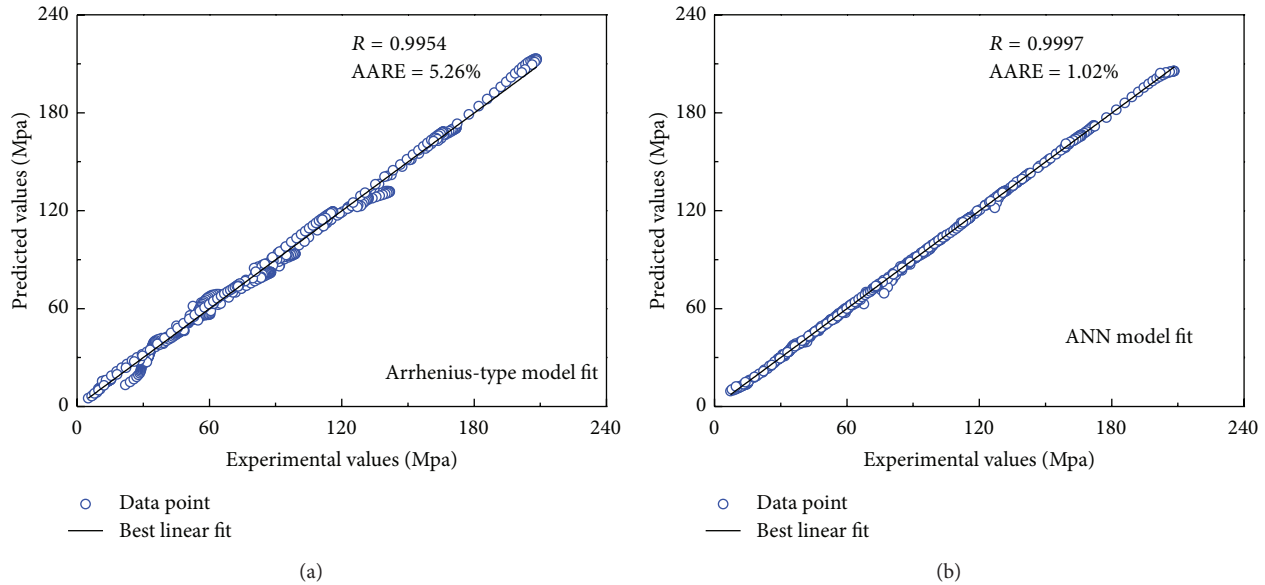


FIGURE 9: Correlation between experimental and predicted flow stress data from (a) constitutive model and (b) ANN model.

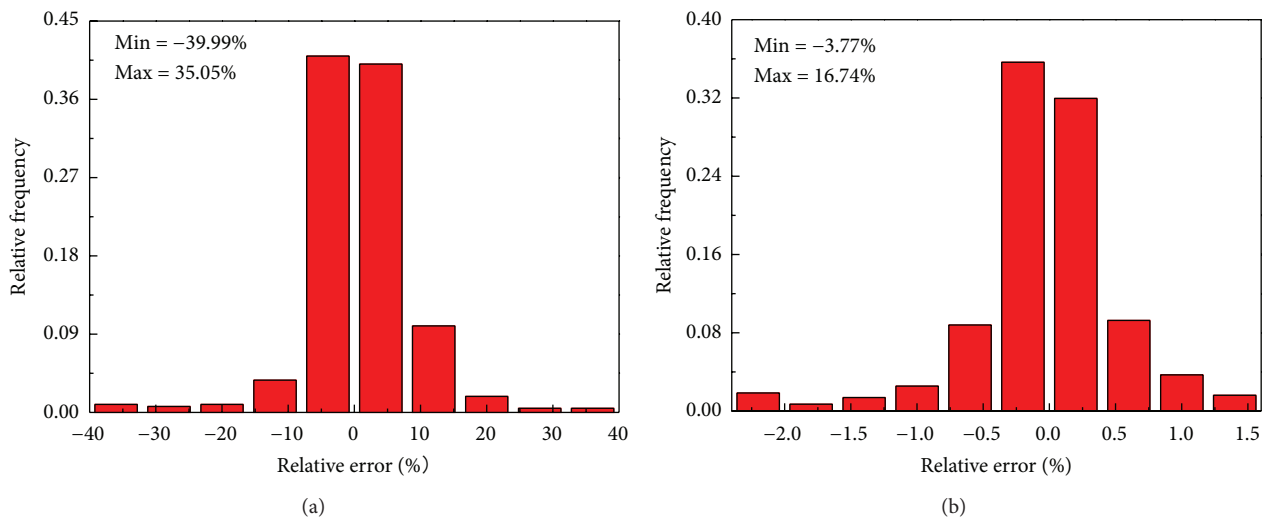


FIGURE 10: Distributions on prediction error by (a) constitutive model and (b) ANN model.

be seen that the flow stress varies from 0 to 200 MPa with increase in the strain rate from 0.01 to 10 s^{-1} and decrease in temperature from 1173 to 1473 K, which indicates that the predictions are well in agreement with the experimental knowledge.

4. Conclusions

The experimental stress-strain data from the isothermal hot compression tests on a Gleeble-1500 thermomechanical simulator, in a wide range of temperatures (1173~1473 K) and strain rates ($0.01\sim 10 \text{ s}^{-1}$), were employed to develop the Improved Arrhenius-type constitutive model and ANN constitutive model for 20MnNiMo alloys. A comparative

study was carried out on their capability to represent the high-temperature deformation behavior of 20MnNiMo alloy. The conclusions can be drawn as follows.

- (1) The correlation coefficient (R) and average absolute relative error (AARE) for the improved Arrhenius-type model are 0.9954 and 5.26%, respectively, while their values for the ANN model are 0.9997 and 1.02%, respectively. Higher R -values and lower AARE-values for the ANN model indicate that it has a good predictability under limited experimental conditions.
- (2) The relative errors (η) of the improved Arrhenius-type model and the ANN model were, respectively, in the range of $-39.99\%\sim 35.05\%$ and $-3.77\%\sim 16.74\%$. As for the former, only 16.3% of the test data set

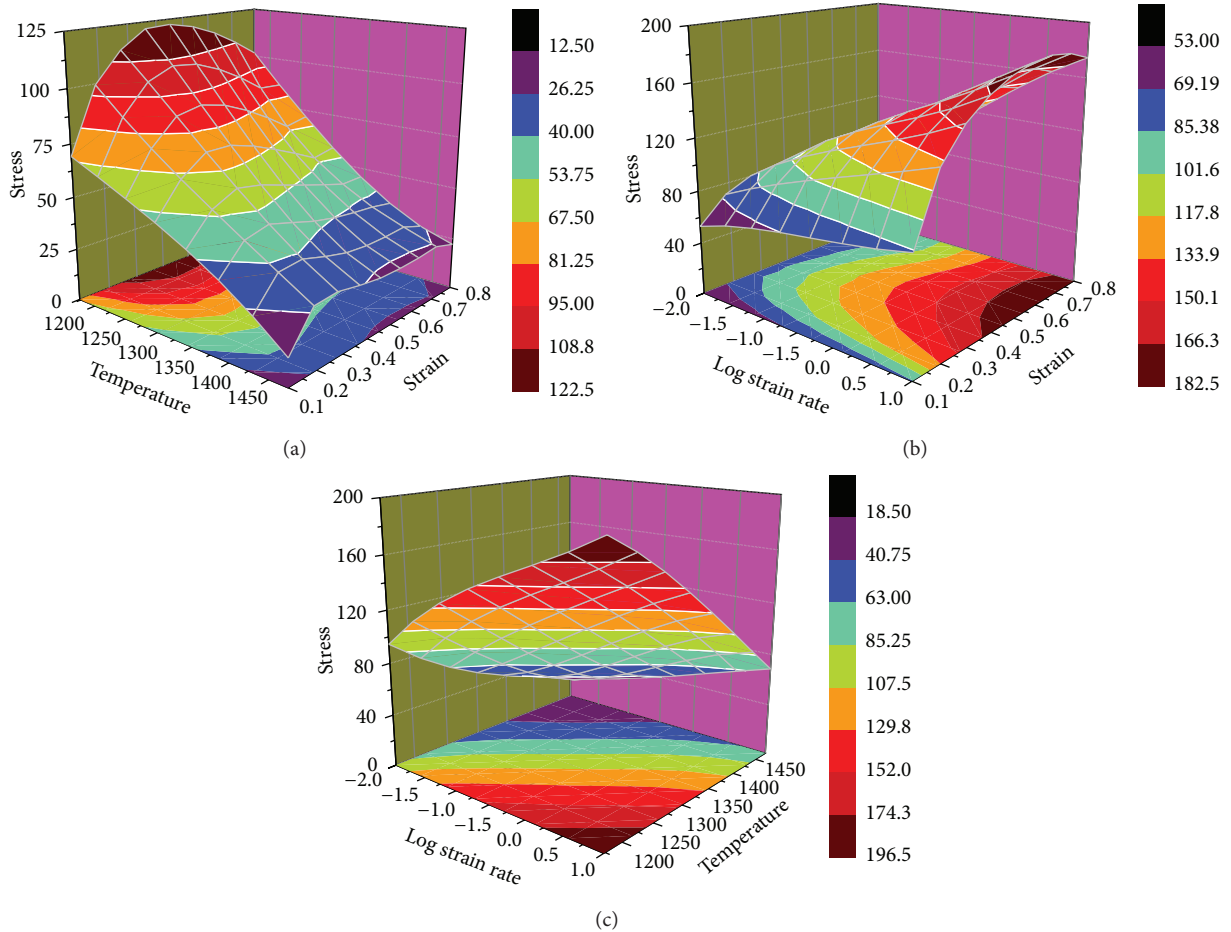


FIGURE 11: ANN model prediction on the relationship of flow stress versus (a) strain and temperature at strain rate of 0.01 s^{-1} (b) strain and log strain rate at temperature of 1273 K (c) log strain rate and temperature at strain of 0.5.

possesses η -values within $\pm 1\%$, while, as for the latter, more than 79% possesses. The results indicate that the ANN model presents a higher predictable ability than the improved Arrhenius-type constitutive model.

- (3) The ANN model for as-cast 20MnNiMo alloy accurately track the experimental data over a wider range of temperatures and strain rates (not only under limited experimental conditions but also outside of experimental conditions). Well-trained ANN models provide fast, accurate, and consistent results, making them superior to the Improved Arrhenius-type constitutive equation. The ANN could also be a good forecast tool to study the high-temperature deformation behavior of other alloys in materials science.

Conflict of Interests

The authors declare that there is no conflict of interests regarding the publication of this paper.

Acknowledgment

This work was supported by National Natural Science Foundation of China (51305469).

References

- [1] M. H. Wang, Y. F. Li, W. H. Wang, J. Zhou, and A. Chiba, "Quantitative analysis of work hardening and dynamic softening behavior of low carbon alloy steel based on the flow stress," *Materials and Design*, vol. 45, pp. 384–392, 2013.
- [2] Y. C. Lin, M.-S. Chen, and J. Zhong, "Constitutive modeling for elevated temperature flow behavior of 42CrMo steel," *Computational Materials Science*, vol. 42, no. 3, pp. 470–477, 2008.
- [3] B. S. Lee, Y. J. Oh, J. H. Yoon, I. H. Kuk, and J. H. Hong, "J-R fracture properties of SA508-1a ferritic steels and SA312-TP347 austenitic steels for Pressurized Water Reactor's (PWR) primary coolant piping," *Nuclear Engineering and Design*, vol. 199, no. 1, pp. 113–123, 2000.
- [4] M. Y. Sun, L. H. Hao, S. J. Li, D. Li, and Y. Li, "Modeling flow stress constitutive behavior of SA508-3 steel for nuclear reactor pressure vessels," *Journal of Nuclear Materials*, vol. 418, no. 1–3, pp. 269–280, 2011.

- [5] S. A. Krishnan, C. Phaniraj, C. Ravishankar, A. K. Bhaduri, and P. V. Sivaprasad, "Prediction of high temperature flow stress in 9Cr-1Mo ferritic steel during hot compression," *International Journal of Pressure Vessels and Piping*, vol. 88, no. 11-12, pp. 501-506, 2011.
- [6] C. Phaniraj, D. Samantaray, S. Mandal, and A. K. Bhaduri, "A new relationship between the stress multipliers of Garofalo equation for constitutive analysis of hot deformation in modified 9Cr-1Mo (P91) steel," *Materials Science and Engineering A*, vol. 528, no. 18, pp. 6066-6071, 2011.
- [7] A. Momeni and K. Dehghani, "Characterization of hot deformation behavior of 410 martensitic stainless steel using constitutive equations and processing maps," *Materials Science and Engineering A*, vol. 527, no. 21-22, pp. 5467-5473, 2010.
- [8] Y. C. Lin and X.-M. Chen, "A critical review of experimental results and constitutive descriptions for metals and alloys in hot working," *Materials and Design*, vol. 32, no. 4, pp. 1733-1759, 2011.
- [9] J. Cai, F. Li, T. Liu, B. Chen, and M. He, "Constitutive equations for elevated temperature flow stress of Ti-6Al-4V alloy considering the effect of strain," *Materials and Design*, vol. 32, no. 3, pp. 1144-1151, 2011.
- [10] J. H. Sung, J. H. Kim, and R. H. Wagoner, "A plastic constitutive equation incorporating strain, strain-rate, and temperature," *International Journal of Plasticity*, vol. 26, no. 12, pp. 1746-1771, 2010.
- [11] F. A. Slooff, J. Zhou, J. Duszczuk, and L. Katgerman, "Constitutive analysis of wrought magnesium alloy Mg-Al4-Zn1," *Scripta Materialia*, vol. 57, no. 8, pp. 759-762, 2007.
- [12] Y.-C. Lin, M.-S. Chen, and J. Zhang, "Modeling of flow stress of 42CrMo steel under hot compression," *Materials Science and Engineering A*, vol. 499, no. 1-2, pp. 88-92, 2009.
- [13] P. Changizian, A. Zarei-Hanzaki, and A. A. Roostaei, "The high temperature flow behavior modeling of AZ81 magnesium alloy considering strain effects," *Materials and Design*, vol. 39, pp. 384-389, 2012.
- [14] O. Sabokpa, A. Zarei-Hanzaki, H. R. Abedi, and N. Haghdadi, "Artificial neural network modeling to predict the high temperature flow behavior of an AZ81 magnesium alloy," *Materials and Design*, vol. 39, pp. 390-396, 2012.
- [15] S. Mandal, P. V. Sivaprasad, S. Venugopal, and K. P. N. Murthy, "Artificial neural network modeling to evaluate and predict the deformation behavior of stainless steel type AISI 304L during hot torsion," *Applied Soft Computing Journal*, vol. 9, no. 1, pp. 237-244, 2009.
- [16] A. K. Gupta, S. K. Singh, S. Reddy, and G. Hariharan, "Prediction of flow stress in dynamic strain aging regime of austenitic stainless steel 316 using artificial neural network," *Materials and Design*, vol. 35, pp. 589-595, 2012.
- [17] G. Z. Quan, W. Q. Lv, Y. P. Mao, Y. W. Zhang, and J. Zhou, "Prediction of flow stress in a wide temperature range involving phase transformation for as-cast Ti-6Al-2Zr-1Mo-1V alloy by artificial neural network," *Materials and Design*, vol. 50, pp. 51-61, 2013.
- [18] Y. Zhu, W. Zeng, Y. Sun, F. Feng, and Y. Zhou, "Artificial neural network approach to predict the flow stress in the isothermal compression of as-cast TC21 titanium alloy," *Computational Materials Science*, vol. 50, no. 5, pp. 1785-1790, 2011.
- [19] Y. Han, G. J. Qiao, J. P. Sun, and D. N. Zou, "A comparative study on constitutive relationship of as-cast 904L austenitic stainless steel during hot deformation based on Arrhenius-type and artificial neural network models," *Computational Materials Science*, vol. 67, pp. 93-103, 2013.
- [20] X. Xiao, G. Q. Liu, B. F. Hu, X. Zheng, L. N. Wang, and S. J. Chen, "A comparative study on Arrhenius-type constitutive equations and artificial neural network model to predict high-temperature deformation behavior in 12Cr3WV steel," *Computational Materials Science*, vol. 62, pp. 227-234, 2012.
- [21] D. Ponge and G. Gottstein, "Necklace formation during dynamic recrystallization: mechanisms and impact on flow behavior," *Acta Materialia*, vol. 46, no. 1, pp. 69-80, 1998.
- [22] G.-Z. Quan, Y. Shi, Y.-X. Wang, B.-S. Kang, T.-W. Ku, and W.-J. Song, "Constitutive modeling for the dynamic recrystallization evolution of AZ80 magnesium alloy based on stress-strain data," *Materials Science and Engineering A*, vol. 528, no. 28, pp. 8051-8059, 2011.
- [23] D. Samantaray, S. Mandal, and A. K. Bhaduri, "A comparative study on Johnson Cook, modified Zerilli-Armstrong and Arrhenius-type constitutive models to predict elevated temperature flow behaviour in modified 9Cr-1Mo steel," *Computational Materials Science*, vol. 47, no. 2, pp. 568-576, 2009.
- [24] G.-Z. Quan, T.-W. Ku, and B.-S. Kang, "Improvement of formability for multi-point bending process of AZ31B sheet material using elastic cushion," *International Journal of Precision Engineering and Manufacturing*, vol. 12, no. 6, pp. 1023-1030, 2011.
- [25] H.-Y. Li, D.-D. Wei, Y.-H. Li, and X.-F. Wang, "Application of artificial neural network and constitutive equations to describe the hot compressive behavior of 28CrMnMoV steel," *Materials and Design*, vol. 35, pp. 557-562, 2012.
- [26] R. H. Wu, J. T. Liu, H. B. Chang, T. Y. Hsu, and X. Y. Ruan, "Prediction of the flow stress of 0.4C-1.9Cr-1.5Mn-1.0Ni-0.2Mo steel during hot deformation," *Journal of Materials Processing Technology*, vol. 116, no. 2-3, pp. 211-218, 2001.
- [27] Y. C. Lin, X. Fang, and Y. P. Wang, "Prediction of metadynamic softening in a multi-pass hot deformed low alloy steel using artificial neural network," *Journal of Materials Science*, vol. 43, no. 16, pp. 5508-5515, 2008.
- [28] C. M. Sellars and W. J. McTegart, "On the mechanism of hot deformation," *Acta Metallurgica*, vol. 14, no. 9, pp. 1136-1138, 1966.
- [29] C. Zener and J. H. Hollomon, "Effect of strain rate upon plastic flow of steel," *Journal of Applied Physics*, vol. 15, no. 1, pp. 22-32, 1944.
- [30] S. Mandal, P. V. Sivaprasad, and S. Venugopal, "Capability of a feed-forward artificial neural network to predict the constitutive flow behavior of as cast 304 stainless steel under hot deformation," *Journal of Engineering Materials and Technology, Transactions of the ASME*, vol. 129, no. 2, pp. 242-247, 2007.
- [31] Y. C. Lin, J. Zhang, and J. Zhong, "Application of neural networks to predict the elevated temperature flow behavior of a low alloy steel," *Computational Materials Science*, vol. 43, no. 4, pp. 752-758, 2008.
- [32] Y. Han, G. Qiao, D. Yan, and D. Zou, "Artificial neural network to predict the hot deformation behavior of super 13Cr martensitic stainless steel," *Materials Science Forum*, vol. 695, pp. 361-364, 2011.